ORIGINAL PAPER

Electrospun polycaprolactone/ZnO nanocomposite membranes as biomaterials with antibacterial and cell adhesion properties

Robin Augustine · Hruda Nanda Malik · Dinesh Kumar Singhal · Ayan Mukherjee · Dhruba Malakar · Nandakumar Kalarikkal · Sabu Thomas

Abstract In the present study we have investigated the effect of zinc oxide (ZnO) nanoparticles on the fiber diameter, fiber morphology, antibacterial activity, and enhanced cell proliferation of the electrospun polycaprolactone (PCL) non-woven membrane. The effect of the ZnO nanoparticle concentration on the fiber diameter and fiber morphology was investigated using a scanning electron microscope (SEM). Fourier transform infrared spectroscopy (FT-IR) analysis was carried out to determine the nature of the interaction between the PCL and the ZnO nanoparticles. We also investigated the mechanical stability and antibacterial activity of the fabricated material. Interestingly, the membranes with ZnO nanoparticles showed enhanced mechanical stability, antibacterial properties, fibroblast proliferation, and improved metabolic activity of the cells. Further, this is the first report regarding the ability of a biomaterial containing ZnO nanoparticles to enhance cell proliferation.

**Keywords** Polycaprolactone · ZnO nanoparticles · Scaffolds · Wound healing · Antimicrobial · Fibroblasts

R. Augustine · N. Kalarikkal (✉) · S. Thomas (✉)
International and Inter University Centre for Nanoscience and Nanotechnology, Mahatma Gandhi University, Kottayam 686 560, Kerala, India
e-mail: nkkalarikkal@mgu.ac.in
e-mail: sabupolymer@yahoo.com

N. Kalarikkal
School of Pure and Applied Physics, Mahatma Gandhi University, Kottayam 686 560, Kerala, India

S. Thomas
School of Chemical Sciences, Mahatma Gandhi University, Kottayam 686 560, Kerala, India

H. N. Malik · D. K. Singhal · A. Mukherjee · D. Malakar
Animal Biotechnology Centre, National Dairy Research Institute, Karnal 132001, India

Introduction
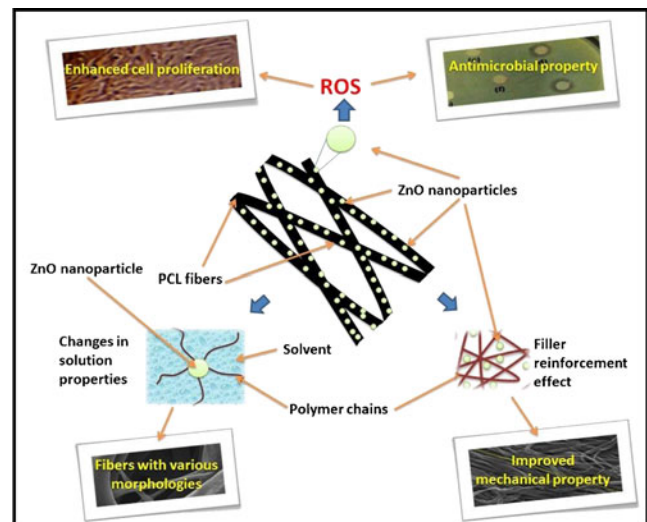
Tissue engineering is a fascinating therapeutic strategy that combines cells, biomaterials, and the cues that induce the differentiation of cells to form tissues into surgically transplantable formats, aimed at the repair, replacement, maintenance or enhancement of tissue function [1, 2]. Tissue engineering scaffolds are three-dimensional backbones that are used for cell proliferation, migration, and differentiation, and that ultimately aid in the formation of the extracellular matrix (ECM) and the desired tissue. The chemical composition, surface energy, roughness, and topography of the top surface of the scaffold, which are in direct contact with biological systems, determines the cell-scaffold interaction [3]. Biological and mechanical properties of porous scaffolds are determined by their morphological characteristics. Specific surface area and porosity are two main morphological parameters of the scaffolds [4]. Fabricating tissue-engineering scaffolds that

exactly mimic the structure of the extracellular matrix at the nanoscale is one of the major challenges in the field of tissue engineering and the development of nanofibers can potentially meet this challenge [5]. Sufficient porosity and pore size are essential to facilitate cell seeding and diffusion throughout the scaffold of both cells and nutrients [6]. According to Oh et al., the optimum pore size and spatial distribution for proper cell growth and tissue regeneration vary with the type of tissue to be constructed [7]. The scaffold should have adequate mechanical properties compatible with those of the tissue at the implantation site or mechanical properties that are sufficient to protect cells from damaging compressive or tensile forces without affecting appropriate molecular signals [8].

The process of electrospinning enables the production of continuous fibers with dimensions on the scale of nanometers or submicrons from a wide range of natural and synthetic polymers [9]. A high surface-area-to-volume ratio and the high porosity on the sub-micrometer length scale make these materials suitable for many biomedical applications [10–14]. Their applicability in regenerative medicine and tissue engineering has significantly increased the amount of research in this arena. For the past few decades, a considerable effort has been made by many researchers to improve the properties of electrospun, polycaprolactone, non-woven mats [11, 15, 16].

Since polycaprolactone (PCL) is biocompatible and biodegradable, it has immense potential as biomaterial for various biomedical applications including tissue engineering scaffolds, wound dressings, hemostats, etc [17–19]. Electrospinning of PCL has been reported in many studies over the past few years. Efforts have been made to improve both the mechanical and morphological features of electrospun-PCL non-woven membranes.

The incorporation of various filler materials like nanoparticles and blending with other polymers have resulted in significant improvement in the overall performance of biomaterials. The major goal of such efforts have been aimed at reducing the fiber diameter, achieving fibers with uniform fiber diameters, and maintaining good mechanical properties. In one study, electrospun PCL fibers incorporated with $CaCO_3$ or HA nanoparticles were fabricated and shown to improve cell attachment [11].

Zinc oxide (ZnO) is an inorganic compound used widely in everyday applications. ZnO is currently listed as a 'generally recognized as safe' (GRAS) material by the Food and Drug Administration and is used as a food additive. Nanoparticles of ZnO and their application in coating systems have attracted a great deal of attention in recent years because of their multifunction properties, especially in terms of antibacterial activity. Li et al. studied the antibacterial and physical properties of poly (vinyl chloride) (PVC)-based film coated with ZnO nanoparticles and found that the particles have a good potential to be used as an active coating system for food packaging [20]. Compression-molded PCL-ZnO nanocomposites are already reported in the literature and are superior to the bare polymer in terms of increased barrier properties and mechanical properties [21]. Microbial invasion and proliferation on biomaterials is a major problem that limits the success of such materials. For these reasons, while designing a material for medical use, it is extremely important to ensure its resistance to microbial attack [22]. The effectiveness of polyurethane membranes with zinc oxide nanoparticles to resist both bacteria and fungi has already been reported [23].

The role of reactive oxygen species (ROS) in cell proliferation and wound healing through the activation of growth factors has been discussed previously [24–28]. The ability of ZnO nanoparticles to generate ROS is also well-established [29–33]. A recent report suggested that ZnO nanoflowers induced the proliferation and migration of endothelial cells and led to the formation of new blood vessels [34].

The element zinc participates in DNA and RNA synthesis, which are directly related to cell replication, which entails the differentiation of cells, including fibroblasts, and cell transcription. Zinc is also essential to enzyme systems that influence cell division and proliferation. [35, 36]. Fujiwara et al. reported that zinc enhances vascular smooth muscle cell proliferation induced by basic and acidic fibroblast growth factors, as well as thrombospondin [37]. Endopeptidases like matrixmetaloproteinases (MMPs), which require zinc for catalytic activity and are capable of digesting ECM and basement membrane components, are important for fibroblast proliferation [38]. The increased expression of MMPs leads to the proteolytic breakdown of the basement membrane and ECM leading to the release of FGFs, which enhances cell proliferation [39]. Sudheesh Kumar et al. reported the use of ZnO nanoparticles containing β-chitin hydrogel bandages with antimicrobial and wound healing properties. The fabricated materials possessed good biocompatibility to human dermal fibroblast cells [40]. Thus, the zinc oxide in its nano-dimensions may have enhanced activity in fibroblast proliferation due to its large surface area and subsequent increased catalytic efficacy.

In the following, we propose the design of novel tissue-engineering scaffolding materials with tunable morphology, high mechanical stability, antibacterial properties, and enhanced tissue proliferation abilities made from electrospun mats of PCL fibers filled with ZnO nanoparticles. This is the first report regarding the ability of biomaterials containing ZnO nanoparticles to enhance the mammalian cell proliferation.

Materials and Methods

Materials

The polycaprolactone (Mw 70,000) used in this study was purchased from Sigma Aldrich, St. Luis, USA. The ZnO

nanoparticles were of an average particle size of 60 nm and purchased from Sigma Aldrich, St. Luis, USA. Acetone was obtained from Merck, Mumbai, India. All the reagents used in this study were of analytical grade quality and therefore used without further purification.

Methods

Electrospinning of Polycaprolactone with ZnO Nanoparticles

Electrospun membranes of PCL, into which we incorporated ZnO nanoparticles of particle size range ~60 nm, were prepared by electrospinning 15 wt.% PCL in acetone. The electrospinning apparatus was assembled by Holmarc, India, and consisted of a syringe pump, a high-voltage power supply, and a 10-ml syringe with an attached 21G-diameter needle. The needle-to-collector distance was maintained at 15 cm with an applied voltage of 18 kV. The feeding rate of the solution was precisely controlled by a syringe pumping system, which was adjusted to a flow rate of 1 ml/h. As a collector, a thin aluminum sheet of 7 cm^2 was attached to the fixed collector, which was grounded properly.

Polycaprolactone solutions with different concentration of ZnO nanoparticles were prepared in acetone. Briefly, a lower concentration range (0.1 to 1 wt.%) and a comparatively higher concentration range (1–6 wt.%) of ZnO nanoparticles were accurately weighed and ultrasonicated for 15 min to properly disperse in acetone. Then, a known quantity of PCL was added to the above solution so that the final solution contained 15 wt.% PCL, and the mixture was stirred with a magnetic stirrer for 12 h to ensure the dissolution of the pellets and proper mixing. About 10 ml of the prepared solutions with different wt% of ZnO nanoparticles were taken in plastic syringes and electrospun individually on aluminum sheets.

Characterization

The fabricated PCL/ZnO nanocomposite membranes were characterized using various techniques like scanning electron microscopy (SEM), energy-dispersive X-ray spectroscopy (EDX), Fourier transform infrared spectroscopy (FTIR), and X-ray diffraction (XRD) analysis. Mechanical properties were also determined using a universal testing machine according to ASTM standards. The antimicrobial property of the fabricated material was evaluated by the disc diffusion method.

Scanning Electron Microscopy

The morphological features of the fabricated membranes were observed by SEM. The neat PCL membrane as well as the PCL/ZnO nanocomposite membranes were carefully sectioned with an approximate size of 3-mm length and 0.5-mm width using a sharp scissor, and then mounted onto an SEM grid. Prior to the examination, each sample was coated with platinum using a JEOL JFC 1600 Autofine coater. A JEOL JSM 6390 scanning electron microscope at 10 kV was used to analyze the samples. The average fiber diameter of each sample was quantified from the SEM image using ImageJ software. Measurements were made at 100 random positions and the average of these measurements gave the diameter of the nanofibers.

Energy-dispersive X-ray Spectroscopy

The presence of ZnO nanoparticles in the polycaprolactone membrane was investigated by EDX analysis using an Oxford Swift ED attached to a JEOL JSM 6390 SEM, based on the energy and intensity distribution of X-ray signals generated by the electron beam striking the surface of the specimen.

Fourier Transform Infrared Spectroscopy

Fourier transform infrared spectroscopy (FT-IR) spectra were obtained with a Perkin Elmer, spectrum 400 FTIR spectrometer. The powders of ZnO nanoparticles, and PCL/ZnO nanocomposite membranes with different wt% of ZnO nanoparticles were subjected to IR analysis. The spectra were collected over a range of 400–4,000 cm^{-1}.

X-Ray Diffraction Analysis

X-Ray diffraction (XRD) was used to understand the crystallinity and the structure of the fabricated materials. XRD was recorded in the 2θ range of 5°–80° using a model D8-Advance of Bruker (Germany), of CuKα radiation, of which the energy was 8.04 keV and the wavelength was 1.54 Å. The applied voltage was 40 kV and the current was 25 mA.

Mechanical Measurements

Tensile tests of the electrospinning nanofibrous membrane were carried out with a Tinus Olsen H50 KT Universal Testing Machine according to the ASTM D 882 standard by applying a 500-N load cell at a crosshead speed of 1 mm/min. All the samples were cut into rectangles with dimensions of 6×1 cm^2 and vertically mounted in between two mechanical gripping units of the tester, leaving a 3-cm gauge length for mechanical loading. The sample thicknesses were measured with an electronic micrometer having a precision of 1 μm. The average values of tensile property were obtained from the results of five tests and expressed as the mean±standard deviation (SD).

Antimicrobial Activity: Disc Diffusion Technique

In vitro antibacterial activity of the PCL/ZnO nanocomposite membranes was evaluated by the disc diffusion method

according to the National Committee for Clinical Laboratory Standards (NCCLS, 2001). Freshly prepared Mueller-Hinton agar was poured into glass petri dishes to get a uniform depth of approximately 4 mm and allowed to cool. *Escherichia coli* and *Staphylococcus aureus* were used as standard organisms for Gram-negative and Gram-positive bacteria respectively. Three to five well-isolated colonies of the same morphological type of both bacteria were selected from an agar plate culture and inoculated into Mueller Hinton Broth media and incubated at 35 °C until they achieved the turbidity of the 0.5 McFarland standards. To standardize the inoculum density, a $BaSO_4$ turbidity standard, equivalent to a 0.5 McFarland standard was used. A sterile cotton swab was dipped into the standardized bacterial suspension. The Mueller-Hinton agar plate was inoculated by streaking the swab over the entire sterile agar surface. The discs of electrospun PCL membranes with various concentrations of ZnO nanoparticles were cut into approximately 6-mm-diameter pieces and placed onto the surface of the inoculated MHA plates. Discs of PCL membranes without nanoparticles were maintained as controls. The plates were incubated at 35 °C overnight to get a confluent lawn of bacterial growth.

The sensitivity of the microorganisms to membranes was determined by measuring the diameter of inhibitory zones on the agar surface around the discs. All the tests were carried out in triplicate. The diameters of the inhibition zones were measured in millimeters.

Fibroblast Attachment and Proliferation

A small piece of tissue was taken from the ear of a goat using an ear puncturing machine. The hairs were removed and the sample was washed three to four times with DPBS (Dulbecco's phosphate-buffered saline). Then, the tissue piece was dissected into very small pieces with a sterile scalpel and washed with DPBS. Pieces of tissue were placed into 6-well dishes containing fibroblast culture medium (DMEM supplemented with 10 % fetal bovine serum). According to the outgrowth of cells, a portion of the tissue pieces was attached and the remaining portion was removed after 2-3 days. These cells formed a confluent monolayer and were used for further subculturing. The medium from the 6-well culture dish was discarded and 0.5 ml of 0.25 % trypsin-EDTA was added to the dish and kept in a 5 % CO_2 incubator for 2 min to disaggregate the cells. The cells were separated by centrifugation at 1,000 rpm for 5 min. The supernatant was discarded, 1 ml of the fresh fibroblast medium was added, and the suspension was plated at the rate of 500 µl into a 25-cm^2 tissue culture flask containing 2 ml of fresh culture medium and incubated in a CO_2 incubator with 5 % CO_2 supply under 38.5 °C. The medium was replaced after each 48 h interval. Fresh passaged fibroblast cells were layered down in the six-well culture dish containing polycaprolactone membranes with different concentrations of ZnO nanoparticles and incubated in an incubator with 5 % CO_2 supply under 38.5 °C for 4 days. After every 12 h, the culture plates were observed under an inverted microscope (No. X51, Olympus, Japan) and images were taken using a CCD (charge-coupled device) camera attached to the microscope.

Cell Proliferation Assay

The effects of the PCL membranes containing different concentrations of ZnO nanoparticles on the in vitro cell proliferation were assayed by XTT (2,3-bis-(2-methoxy-4-nitro-5-sulfophenyl)-2H-tetrazolium-5-carboxanilide) assay according to the manufacturer's instruction (XTT cell proliferation assay kit, catalog No. 10010200, Cayman Chemical Company, MI, USA) with some minor modifications. XTT assay is used to assess cell viability as a function of redox potential. Actively respiring cells convert the water-soluble XTT to a water-soluble, orange colored formazan product. Briefly, medium from the six-well culture dish containing membranes was discarded and 0.5 ml of 0.25 % trypsin-EDTA was added to the dish and kept in a 5 % CO_2 incubator for 2 min to disaggregate the cells. The cells were pelleted by centrifugation at 1,000 rpm for 5 min and the supernatant was discarded. The fresh fibroblast medium was added and the suspension was plated in a 96-well plate at a density of 0.5×10^5 cells/well in 100 µl of culture medium for 24 h at 37 °C in a CO_2 incubator. Then, 10 µl of the reconstituted XTT mixture was added to each well and mixed gently for 1 min in an orbital shaker. The cells were incubated at 37 °C in a CO_2 incubator for 2 h. The absorbance of each sample was measured at a wavelength of 450 nm in a NanoQuant microplate reader.

The results from the three individual experiments were averaged, expressed as the mean±standard deviation (SD) and statistically analyzed using a *t*-test. A p value less than 0.05 was considered statistically significant.

Results and Discussion

Effect of ZnO Concentration on Fiber Morphology

Analyzing the effect of ZnO nanoparticles on the fiber morphology and structure revealed the spider web structure of the membranes (Figs. 1, 2, 3, 4, 5, 6, 7, 8, 9, 10 and 11). It may be observed from the micrographs that the resulting PCL and PCL-ZnO nanocomposite fiber membranes are almost uniform in fiber diameter and are highly porous.

The effect of ZnO nanoparticles of various concentrations, a lower range of 0.1–0.9 wt.%, and a higher range of 1–6 wt.% significantly changed the fiber morphology provided that other experimental parameters remained constant. In Figs. 1–11, these morphological changes are clearly observable. Figure 1
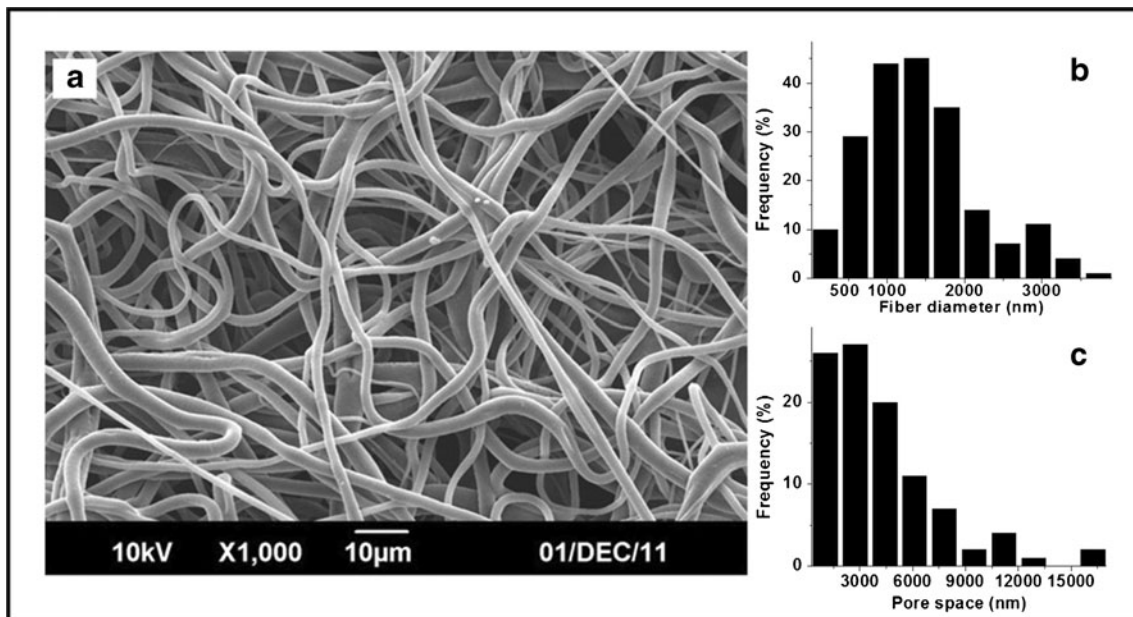
Fig. 1 Scanning electron micrograph of electrospun neat polycaprolactone membrane (**a**), fiber diameter distribution (**b**), and the pore space distribution (**c**)

shows the SEM image of a neat PCL membrane where the surface of individual fibers is very smooth. As the ZnO nanoparticle content in the fibers increases, the surface of fibers becomes rougher due to the agglomerates of ZnO nanoparticles. From 2 wt.% ZnO concentration and onward, the effect is very evident (Figs. 6, 7 and 8), which was in agreement with the results obtained by Patcharaporn et al [11].

Some special morphological features like highly interconnected fibers (Fig. 9) and individual fibers with secondary pores (Fig. 11) were also observed. These features can be explained in terms of the changes in the viscosity of the spinning solution. The interconnected fiber formation occurs when the fibers dry, only after reaching them on the collector. Many other studies also reported observing the secondary pore formation on the individual fibers [41, 42]. This might be due to the breath figure formation, which is directly related to ambient factors like temperature, viscosity of the solution, nature of the solvent, and humidity. Fast evaporation of highly-volatile solvents like acetone from the surface of ejaculated polymer solution makes it cold and leads to the
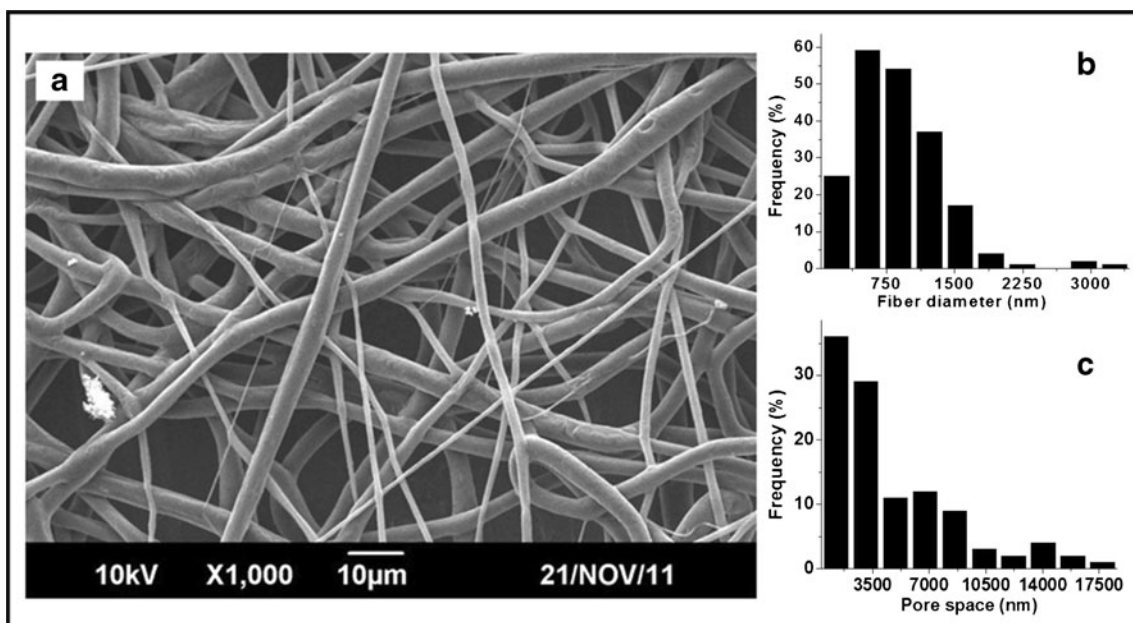

Fig. 2 Scanning electron micrograph of electrospun polycaprolactone membrane with 0.2 wt.% ZnO nanoparticles (**a**), fiber diameter distribution (**b**), and the pore space distribution (**c**)
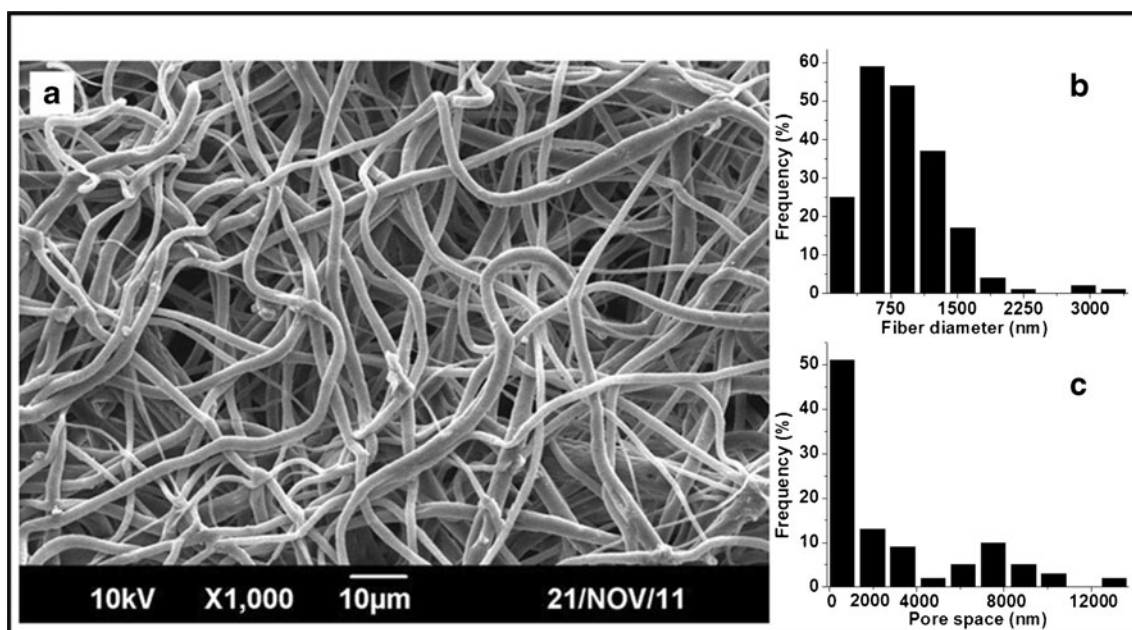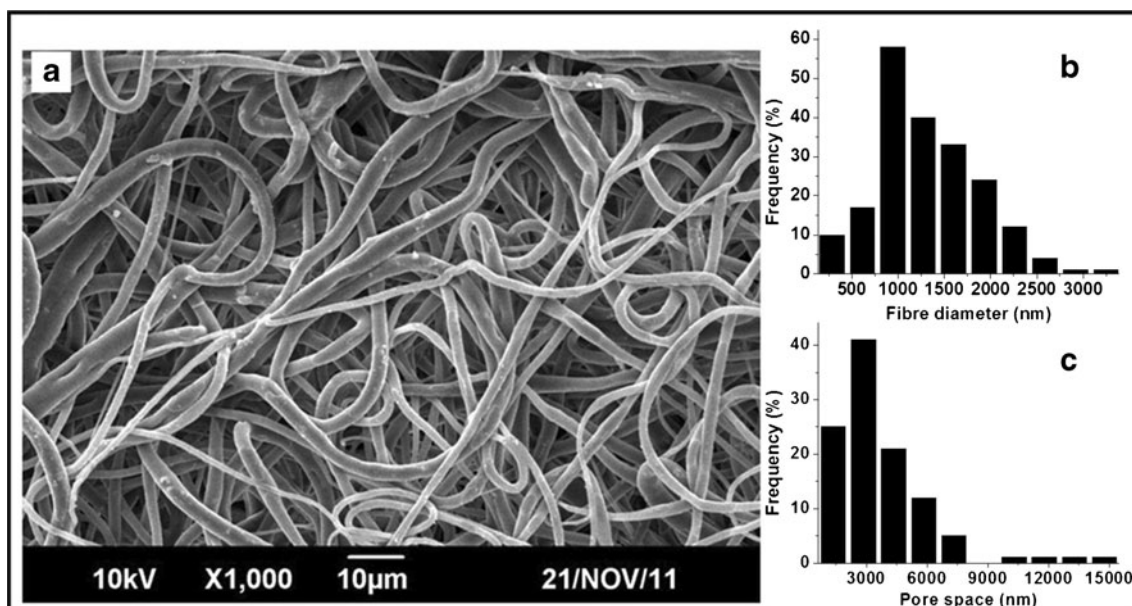
Fig. 3 Scanning electron micrograph of electrospun polycaprolactone membrane with 0.5 wt.% ZnO nanoparticles (**a**), fiber diameter distribution (**b**), and the pore space distribution (**c**)

condensation of water vapor on the surface. During the evaporation of condensed water, droplets from the surface of fibers leave an imprint on the surface, reported as breath figures, which have been extensively studied by various other researchers [42–47].

The challenges of particle dispersion and agglomeration were encountered during the electrospinning in our study, when the ZnO nanoparticle loading was increased above

6 wt.%. At this concentration, formation of the continuous polymer solution jet and subsequent fiber formation became difficult due to the high viscosity of the solution.

Effects of ZnO Nanoparticles on Fiber Diameter

The fiber diameter of the electrospun submicron fibers was observed by SEM and calculated using ImageJ software.

Fig. 4 Scanning electron micrograph of electrospun polycaprolactone membrane with 0.8 wt.% ZnO nanoparticles (**a**), fiber diameter distribution (**b**), and the pore space distribution (**c**)
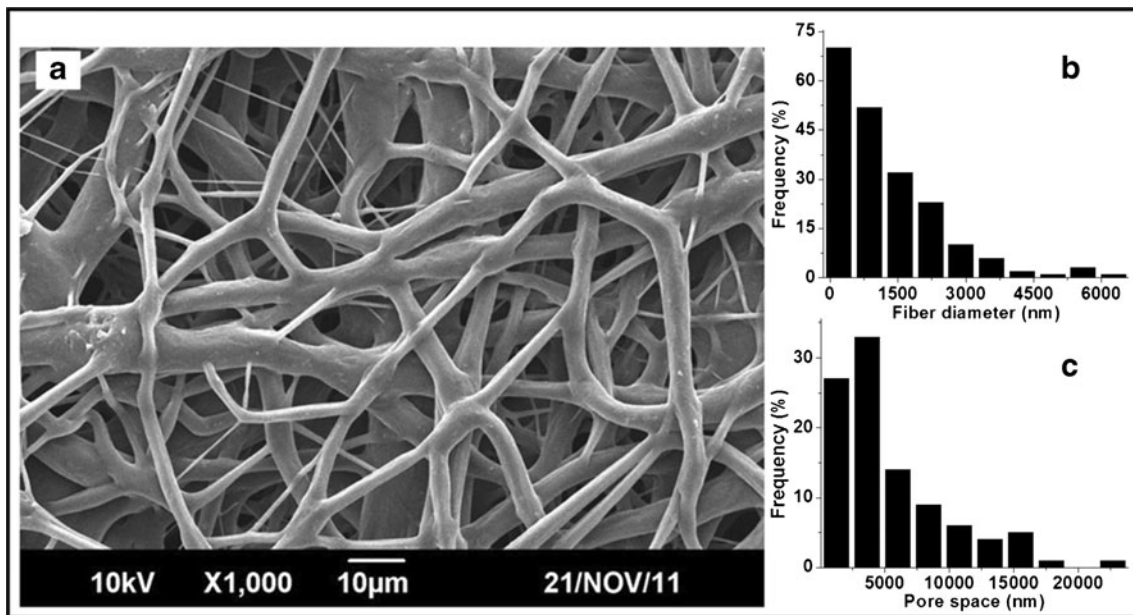
Fig. 5 Scanning electron micrograph of electrospun polycaprolactone membrane with 1 wt.% ZnO nanoparticles (**a**), fiber diameter distribution (**b**), and the pore space distribution (**c**)

Figure 1 shows SEM micrographs of the electrospun neat PCL without ZnO nanoparticles. The fiber diameters, as calculated from the SEM micrographs, are found to be in the average range of 2,500 nm for neat PCL. In the case of PCL-ZnO nanocomposites, as the nanoparticle concentration increased, the fiber diameter was reduced up to 1 wt.% concentration (Fig. 12). After that particular limit, the fiber diameter seemed to increase. Up to 1 wt.% of ZnO nanoparticles, the fiber diameter was continuously reduced and the smallest fibers were obtained at a ZnO nanoparticle concentration of 0.4 wt.% (Average fiber diameter 1,340 nm).

It is well-known that the overall tension in the fibers depends on the self-repulsion of the excess charges on the
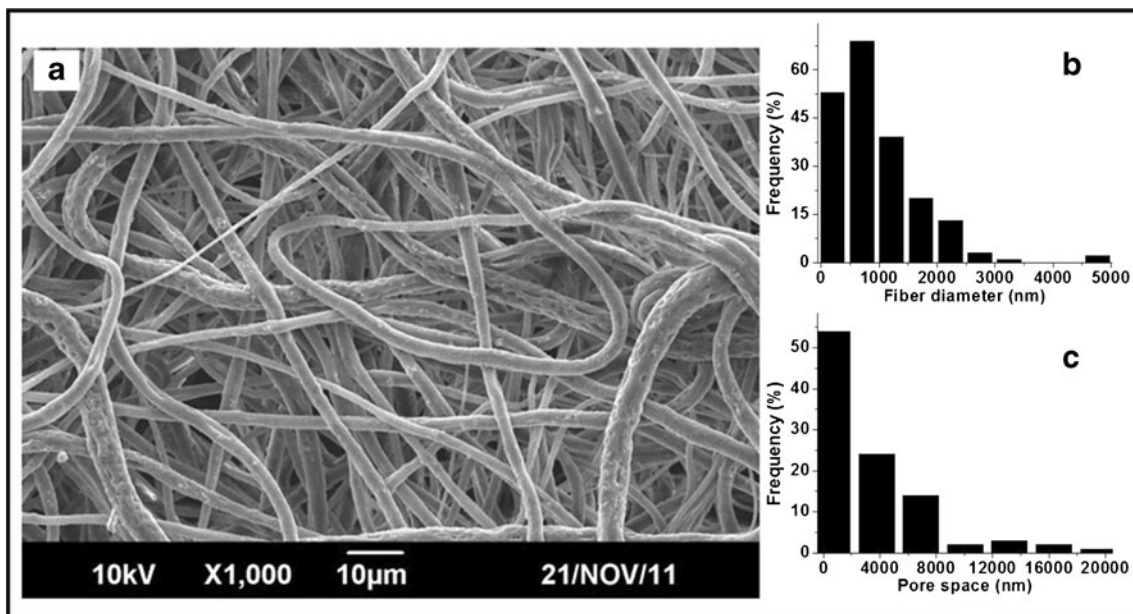

Fig. 6 Scanning electron micrograph of electrospun polycaprolactone membrane with 2 wt.% ZnO nanoparticles (**a**), fiber diameter distribution (**b**), and the pore space distribution (**c**)
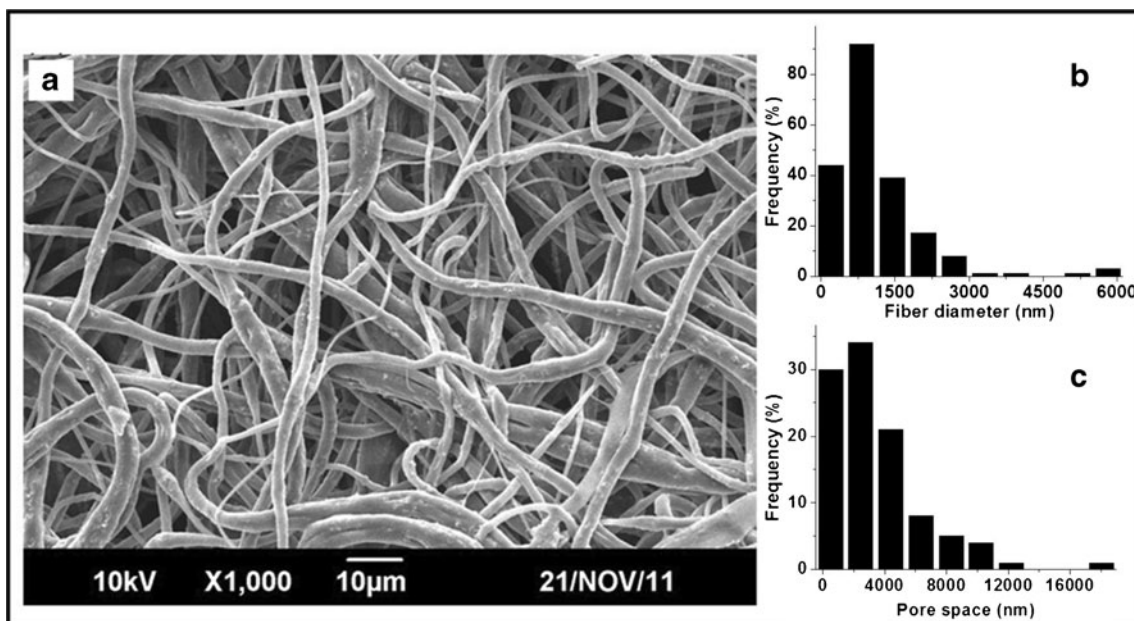
Fig. 7 Scanning electron micrograph of electrospun polycaprolactone membrane with 4 wt.% ZnO nanoparticles (**a**), fiber diameter distribution (**b**), and the pore space distribution (**c**)

jet. The addition of ZnO nanoparticles resulted in the accumulation of a higher charge density on the surface of the ejected jet during the process of electrospinning, and the overall electric charges carried by the electrospinning jet significantly increased [48]. As the charges carried by the jet increased, higher elongation forces that could overcome the self-repulsion were brought down to the jet under the electrical field. Thus, as the charge density increased, the diameter of the final fibers became substantially smaller and the diameter

distribution of fibers became narrower [49]. At higher concentrations of the filler, the viscosity of the solution tended to increase, which led to the apparent increase in fiber diameter [50–52].

Energy-dispersive X-ray Spectroscopy (EDX)

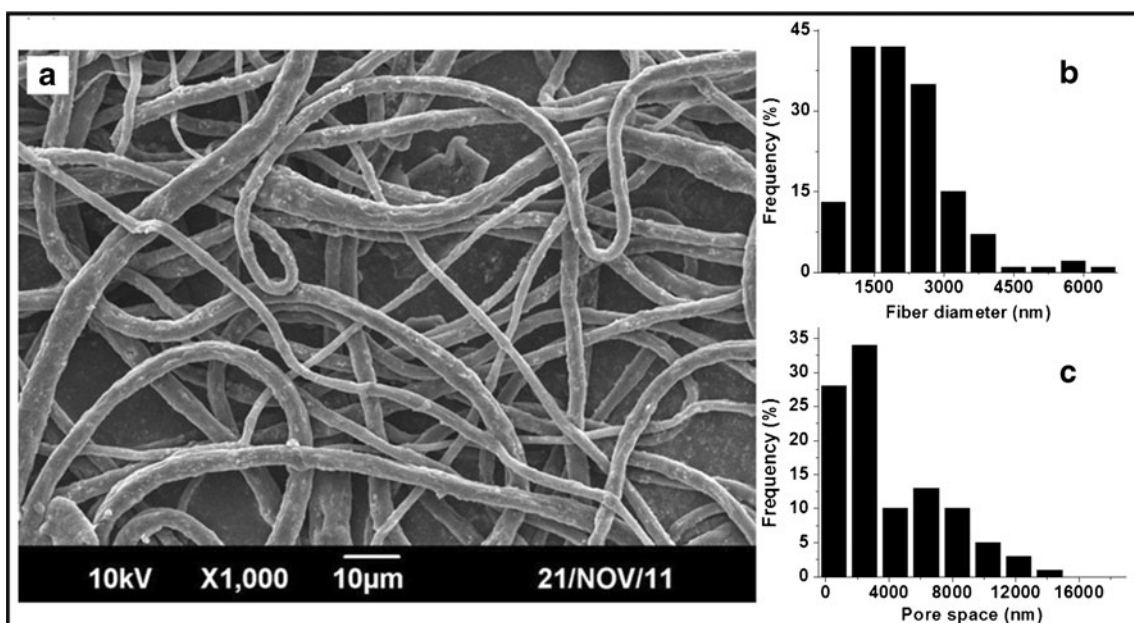The EDX spectrum of PCL and PCL/ZnO nano-composite membranes confirmed the presence of the ZnO nanoparticles

Fig. 8 Scanning electron micrograph of electrospun polycaprolactone membrane with 6 wt.% ZnO nanoparticles (**a**), fiber diameter distribution (**b**), and the pore space distribution (**c**)

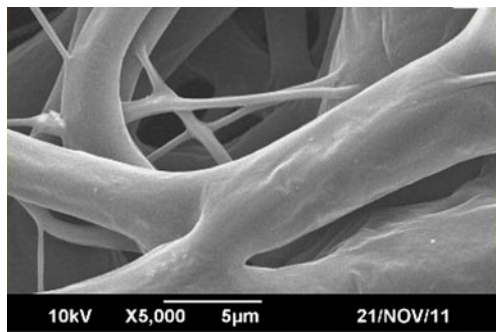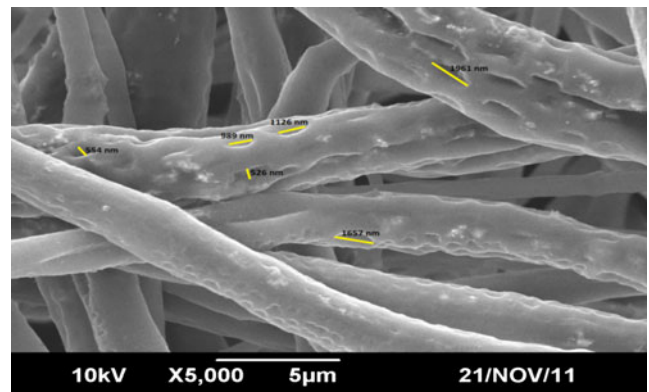**Fig. 9** Interconnected fiber web formed at 1 wt. v% of ZnO nanoparticle concentration

Fig. 11 SEM image of secondary pore formation on fibers at 2 wt.% of ZnO nanoparticle concentration

trapped within the PCL matrix. It also confirmed that the ZnO nanoparticles reached the collector along with the polymer solution during the electrospinning process. Spectra of neat PCL membrane and ZnO nanoparticle-incorporated PCL membranes at varying filler content are shown in Fig. 13. In the case of neat PCL, there are some sharp, low-energy peaks that correspond to the elements carbon and oxygen (Fig. 13a), whereas, in the case of PCL/ZnO composite membranes, three additional peaks could be observed at the energy levels 1 keV, 8.5 keV, and 9 keV, which are the characteristics of zinc. While using 0.2 wt.% ZnO nanoparticle concentration, the peak intensities corresponding to zinc seemed to be very low, and one at the 9.5 Kev level could not be detected. This can be attributed to the fact that elements in low abundance will generate X-ray peaks that may not be resolvable from the background radiation. Moreover, there was a remarkable increase in the intensity of the three characteristic peaks of zinc, as well as one peak of oxygen as we increased the ZnO nanoparticle content from 0.2 to 6 wt.% (Fig. 13b–f).

FT-IR Analysis of the Fabricated Membrane

FT-IR analysis of polycaprolactone/ZnO nanocomposite membranes revealed the incorporation of ZnO into the PCL

matrix. Figure 14 shows the FT-IR spectra of ZnO, polycaprolactone, and PCL/ZnO nanocomposites. FT-IR spectrum of neat PCL shows an intense peak at 1,721 cm^{-1}, which is due to the presence of the ester carbonyl group that corresponds to the –CO (stretching) in the PCL polymer. The peaks at 2,869 and 2,940 cm^{-1} are related to the C–H bond of saturated carbons. The ZnO/polycaprolactone composite and polycaprolactone alone presented the same spectra in the wave number range of 700–3,100 cm^{-1}, while the peak located at 500–700 cm^{-1} is attributed to the stretching of the Zn–O bond.

The FTIR spectrum of ZnO has shown nearly 100 % transmittance. The neat PCL has around 94 % transmittance. Interestingly, the composite has a transmittance range in between that of pure ZnO nanoparticles and neat PCL. As the ZnO content in the composite increased, transmittance of almost all the peaks other than those in the range 500–700 cm^{-1} tended to increase. Furthermore, the decrease in the intensity of the carbonyl stretching vibrations at 1,718-1,721 cm^{-1} indicates the interaction between the carbonyl
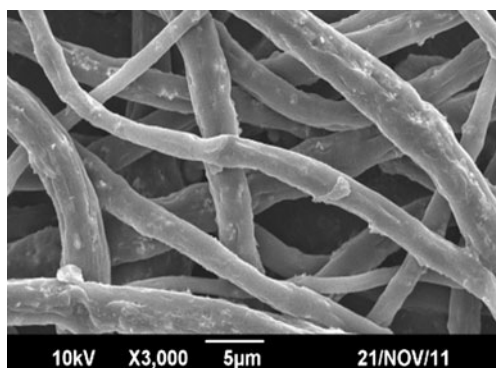

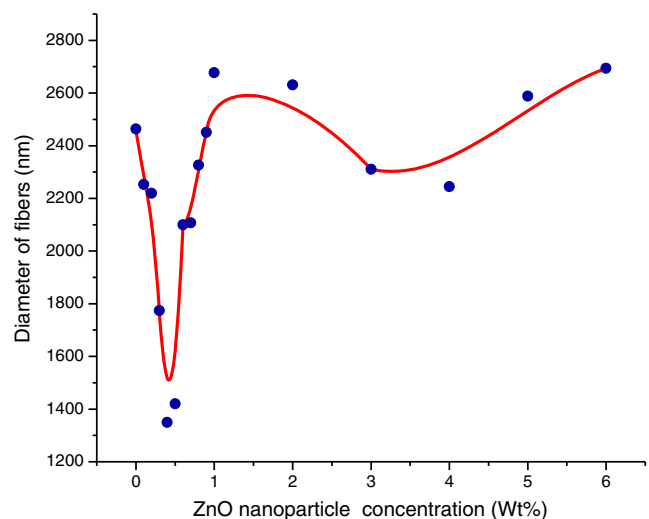**Fig. 10** Formation of aggregates of ZnO nanoparticles on PCL fibers at 6 wt.% ZnO nanoparticle content

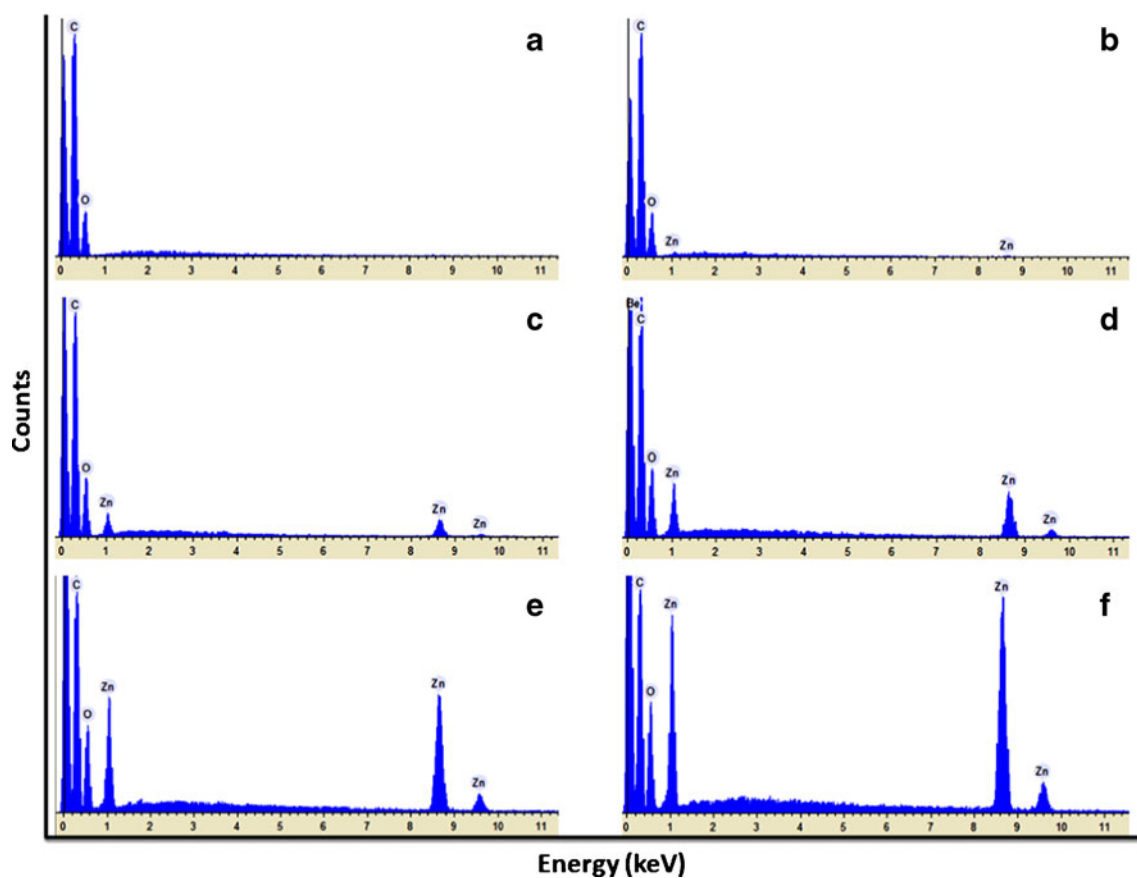**Fig. 12** Effect of ZnO concentration on the fiber diameter

Fig. 13 EDX (Energy-dispersive X-ray spectrum) of neat PCL membrane (**a**), PCL membranes with 0.2 wt.% (**b**), 1 wt.% (**c**), 2 wt.% (**d**), 4 wt.% (**e**) and 6 wt.% (**f**) ZnO nanoparticle concentrations

groups of PCL with ZnO nanoparticles. This physical inter-action may weaken the covalent C=O double bond. This might be the reason for the decrease of intensity of the peak

at 1,718-1,721 cm^{-1}. Additionally, there was a small shift in the peak position to a lower energy level as the concentration of ZnO nanoparticles increased (Fig. 14(b)), revealing the
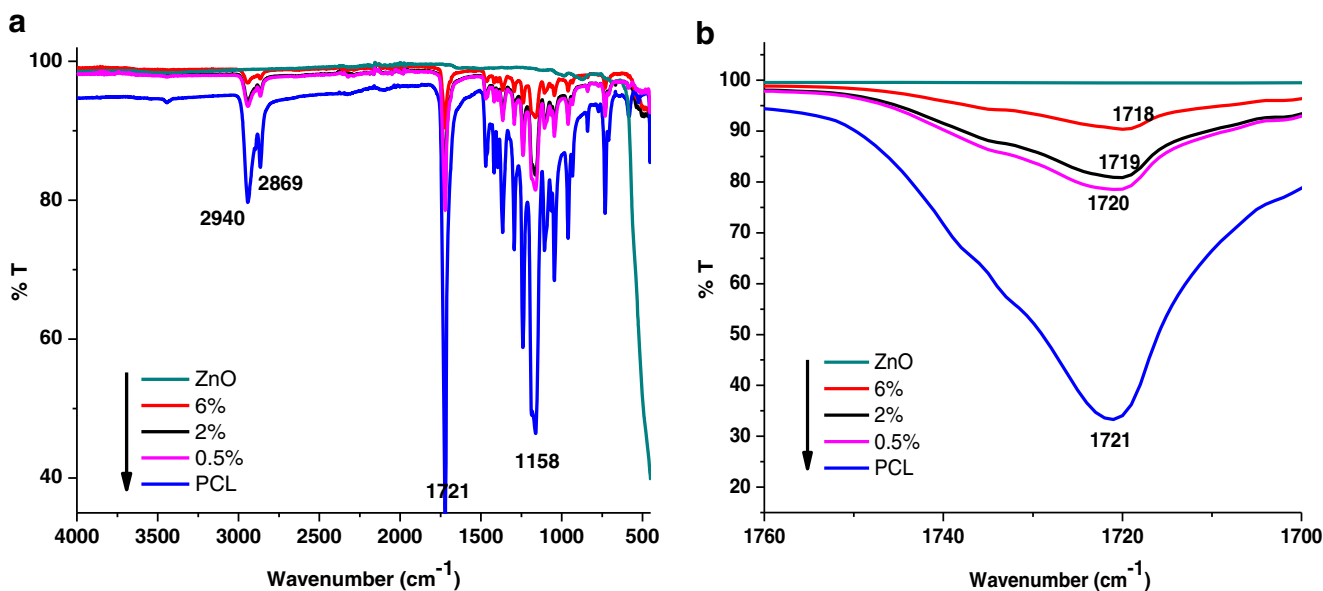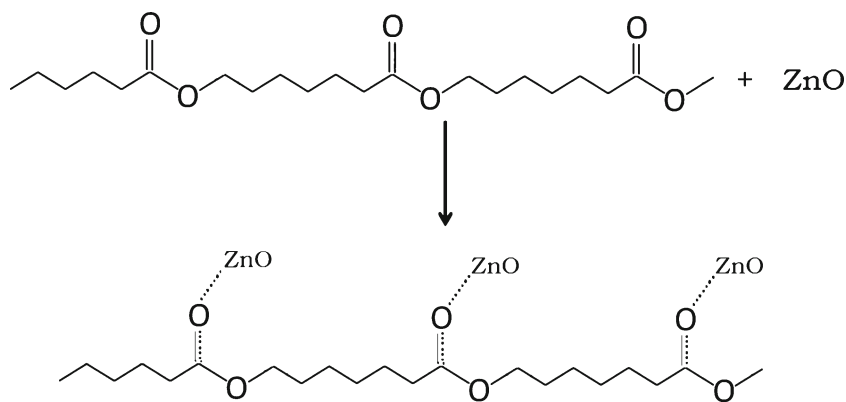

Fig. 14 FT-IR spectra of neat PCL, ZnO nanoparticles and the composites of both at varying concentrations of ZnO nanoparticles (**a**). Decrease in the intensity of carbonyl vibrations as the ZnO concentration increases (**b**)

Scheme 1 Diagrammatic representation of the interaction of ZnO nanoparticles with PCL chains

X-ray Diffraction Analysis

The effect of ZnO nanoparticles on the crystalline behavior of electrospun polycaprolactone nanofibers was studied by X-ray diffraction (XRD) analysis. The XRD patterns of the neat PCL membrane and ZnO/PCL nanocomposites are shown in Fig. 15.

The results show that the neat PCL membrane contains three distinct reflections at the Bragg angles of about 21.4,

interaction of ZnO nanofillers with the PCL polymer chains. The interaction might be of physical interactions like Vander Waals forces that probably weaken the strength of the ester bond present in PCL, as shown in Scheme 1.

22.0 and 23.7°, corresponding to the (110), (111), and (200) planes of the orthorhombic crystal structure, respectively [21]. The behavior of the dominant crystalline phase in the PCL/ZnO nanocomposites can be predicted from the XRD patterns in order to indicate the change in the dominant crystalline phase with increasing ZnO content. The crystallinity of polymer matrix usually tends to decrease with the addition of nanofillers, and the amorphous phase increases accordingly [53]. In the case of neat PCL, a clear and sharp diffraction peak is evident at $2\theta=21.2°$, 22.0°, and 23.7°, illustrating the semi-crystalline nature of neat PCL. The addition of filler up to 1 wt.% resulted in no significant variation in the diffraction peaks. However, compared with the neat PCL nanofiber membrane, the diffraction peaks broaden as a result of the reduction in crystallinity and the increase in amorphous nature at higher filler content, which might be due to the complexation between polymer and filler [12]. At a ZnO content of 0.2 wt.% in the PCL matrix, the peak area of all the three crystalline peaks slightly decreased, but increasing the ZnO content to more than 1 wt.% resulted in a drastic change in crystalline behavior. This clearly indicates that the crystalline nature of PCL decreased with increasing ZnO concentration to a great extent. This was due to the fact that the mobility of the PCL chain was restricted by ZnO aggregates, such that it was difficult for PCL to crystallize, resulting in a decrease in the crystallinity of PCL in the composite. Lim et al. reported that electrospun PCL nanofibers with smaller diameters have a higher degree of molecular orientation, crystallinity, stiffness, and strength. According to their work, nanofiber diameter and the resulting crystalline morphology are influenced by whether complete crystallization of polymer chains took place before or after the electrospinning jet reached the collector. The former result leads to the formation of smaller fibers with fibrillar structure and aligned lamellae, but the latter leads to the formation of a misaligned lamellar structure [54]. A similar trend can be observed here as well. At a lower concentration of ZnO, a nonwoven membrane with smallest diameter is obtained
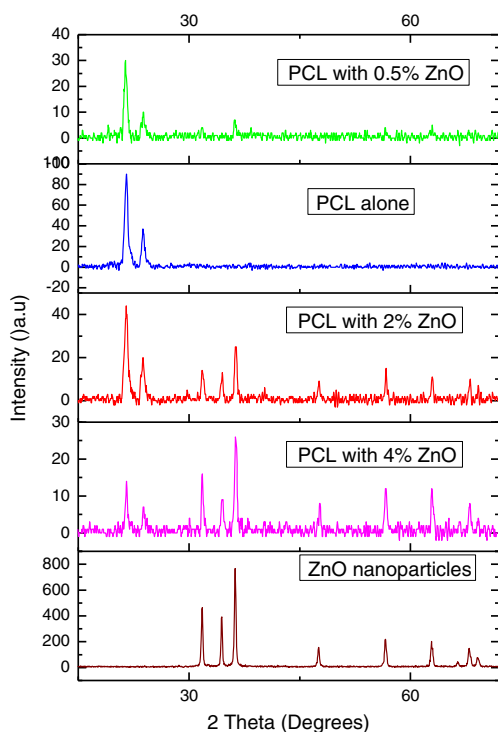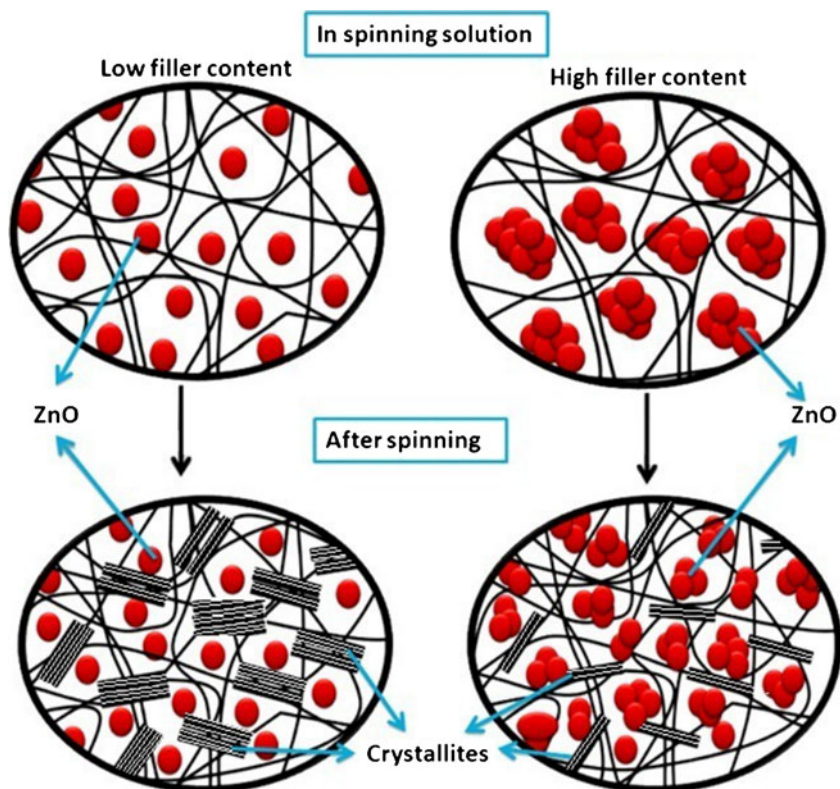

Fig. 15 XRD analysis of PCL and PCL/ZnO nanocomposites

**Scheme 2** Mechanism of crystallization of PCL after electrospinning in the presence of ZnO nanofillers

(Fig. 12). Up to 1 % ZnO concentration, smaller fibers were obtained compared to those seen in the neat PCL and these fibers showed a comparatively higher crystallinity than at the higher ZnO content where larger fibers were obtained. A diagrammatic representation of the dispersion of ZnO nanoparticles at lower and higher concentrations are depicted in Scheme 2.

Mechanical Properties

The typical tensile stress–strain curves for electrospun PCL/ZnO nanocomposites are presented in Fig. 16.

From the figure, it is clear that by adding a lower ZnO nanoparticle content, the tensile strength of the membranes increased with increasing ZnO content. The increase of the

Fig. 16 Stress–strain curves of PCL and PCL/ZnO nanocomposites with varying concentrations of ZnO nanoparticles
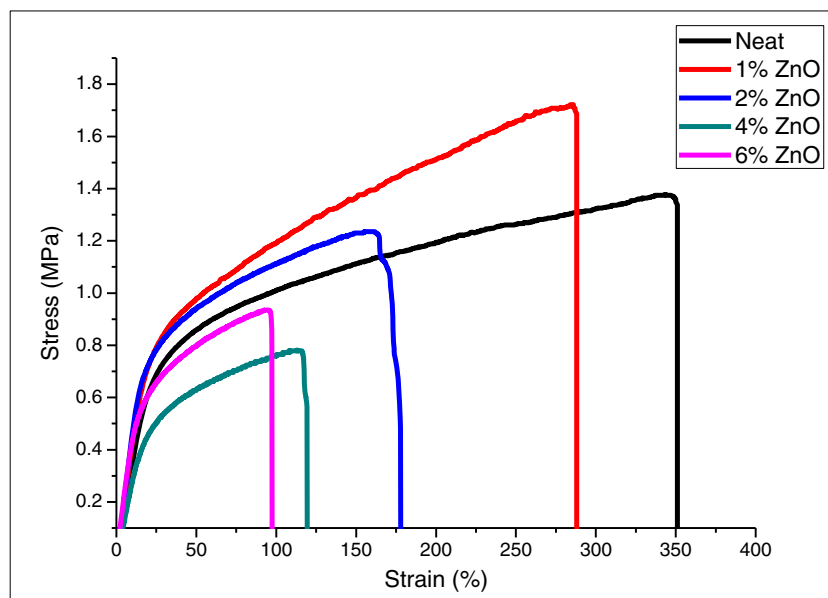
tensile modulus of the composite proceeds linearly with the ZnO content up to 1 wt.%, while further increasing the ZnO nanoparticle content (2, 4, and 6 wt.%) led to a decrease in tensile strength of the PCL/ZnO nanocomposite membranes. The smaller weight percentage of the ZnO nanoparticles resulted in a strong reinforcing effect, increasing the tensile modulus and inhibiting polymer drawing. The PCL membrane with 1 wt.% ZnO nanoparticles showed superior tensile strength compared with the neat PCL membrane. At higher ZnO content, the tensile behavior reverses and all the mechanical properties seemed to be retarded. This is due to the fact that nanoparticles have high surface energy and are easy to aggregate, which leads to the poor dispersion of them in polymer matrix. As the content of ZnO increased, this tendency was also increased and the aggregates of ZnO formed in the polymer matrix acted as stress concentration centers that prevented the stress transfer from the polymer matrix to the fillers. Thus, at lower percentages of ZnO content, there will be a uniform dispersion of ZnO in PCL polymer matrix, provided there is more uniform stress distribution, minimized formation of stress-concentration centers, increased interfacial area for stress transfer from the polymer matrix to the fillers, and good mechanical properties [54, 55]. Also, the PCL–ZnO nanofibers with less than 1 wt.% filler content showed the finest fiber sizes, and since many nanofibers form membranes, they can thus provided more contact and stronger cohesion among the fibers. Furthermore, as mentioned earlier, increasing the filler content above 1 wt.% led to a drastic decrease in the crystallinity of the polymer. Crystalline polymers are stronger than amorphous ones. Electrospun polycaprolactone nanofibers with smaller diameters have a higher degree of crystallinity, molecular orientation, strength, and stiffness, but lower ductility [54]. A similar trend has been observed in our investigation for ZnO concentration of up to 1 wt.%, in which range the non-woven membrane with the smallest diameter was obtained (Fig. 12). From the tensile testing (Table 1) it is clear that the modulus was higher for this sample. Maximum elongation (%), modulus, and break stress also showed similar trends. Nanofibers had a randomly

oriented distribution in the membrane. When the membrane was uniaxially stretched, only fibers along the elongation direction were stretched; fibers of the other direction generally slid and turned to the elongation direction, and then also stretched during this process (Fig. 17).

Thus, the observed irregularities in the stress–strain curve and the modulus might be due to this random orientation of fibers [54]. These results indicated that nanocomposite fibers with lower ZnO content, less agglomeration, and finest fiber sizes would produce fibers with better mechanical properties.

Antibacterial Properties

The antibacterial activity of the ZnO nanoparticle-filled polycaprolactone fiber mats was assessed by observing their activity (based on the disc diffusion method) against both Gram-negative (*Escherichia coli*) and Gram-positive (*Staphylococcus aureus*) bacteria. The activity of the neat PCL membranes against these bacteria was used as a control. The results of the antimicrobial activity analysis are shown in Fig. 18 and Table 2.

From Fig. 18, it is clear that the fabricated membrane had good antimicrobial activity against both *E. coli* and *S. aureus*. According to the results obtained, neat PCL membranes and fiber mats with a ZnO nanoparticle content less than 5 wt.%, showed no activity against the tested bacteria. The PCL membrane containing 5 % ZnO nanoparticles showed statistically significant antibacterial activity with an inhibitory zone diameter of 8.76 ± 1.2 ($P=0.0278$) and 9.98 ± 0.6 ($P=0.0082$) against *E. coli* and *S. aureus*, respectively. The PCL membrane containing 6 % ZnO nanoparticles showed an inhibitory zone diameter of 9.81 ± 0.8 ($P=0.0095$) and 10.22 ± 1.3 ($P=0.0067$) against *E. coli* and *S. aureus*, respectively. The antimicrobial activity was evident only with the 5 and 6 wt.% of ZnO nanoparticles. This was due to the fact that at lower concentrations, the nanoparticles were trapped inside the polymer matrix and thus, those in direct contact with bacterial cells were very few in number. The antibacterial activity of the ZnO

Table 1 Mechanical properties of electrospun PCL/ZnO nanoparticle composite membrane

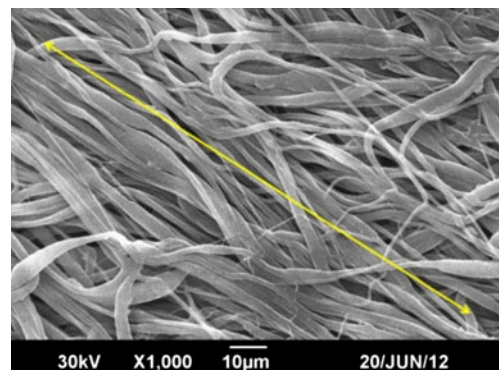| Sample	Filler concentration Wt.%	Break stress (MPa)	Maximum elongation (%)	Modulus (MPa)
1	0	1.40 ± 0.21	342 ± 11	3.70 ± 0.23
2	0.5	1.53 ± 0.12	280 ± 6	4.25 ± 0.15
3	1	1.60 ± 0.23	283 ± 8	5.52 ± 0.21
4	2	1.17 ± 0.12	170 ± 5	4.28 ± 0.12
5	4	0.93 ± 0.04	120 ± 9	3.73 ± 0.2
6	6	0.98 ± 0.11	112 ± 8	3.78 ± 0.21

Fig. 17 Sliding and orientation of individual fibers in the elongation direction during the uniaxial tensile test. *Arrow mark* denotes the direction of applied stress

Fig. 18 Plates showing the antibacterial activity of the fabricated PCL membranes with different concentrations of ZnO nanoparticles against *E. coli* (plate (**a**)) and *S. aureus* (plate (**b**)). In both plates are 2 wt.% (**a**), 3 wt.% (**b**), 4 wt.% (**c**), 5 wt.% (**d**), and 6 wt.% (**e**) ZnO nanoparticles, and PCL membrane alone (**f**)
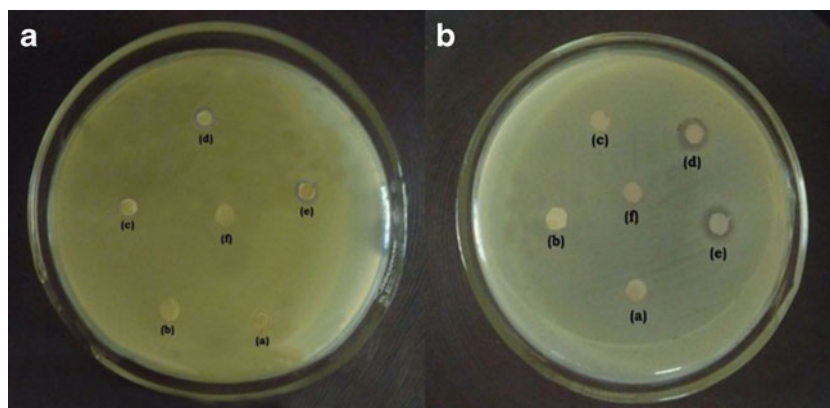
nanoparticles occurs only if the nanoparticles are in direct contact with bacterial cell wall. Further, in the disc diffusion method the antibacterial agent should be able to diffuse into the agar medium to show the antibacterial activity. At higher concentrations of ZnO nanoparticles, the interaction between the polymer matrix and the filler will be apparently low due to higher filler-filler interactions. Thus, there will be more freedom for the entrapped nanoparticles to diffuse into the agar medium and maintain a minimum concentration of ZnO to effectively inhibit bacterial growth. The antibacterial activity of the ZnO/PCL membranes was higher against *S. aureus* than against *E. coli*. Reddy et al. have reported similar results for ZnO nanoparticles [56]. The reason for such an observation could be explained in terms of the difference in the cell wall structure of these bacteria. The outer cell membrane of Gram-negative bacteria contains lipopolysaccharide in its outer leaflet and phospholipids in the inner leaflet. But Gram-positive bacteria lack such a lipopolysaccharide layer. Selahattin et al. proposed that the higher susceptibility of Gram-positive bacteria against ZnO nanoparticles could be related to differences in cell wall structure, metabolism, cell physiology, or the degree of contact points [57]. Many researchers have reported that the antibacterial activity of zinc oxide could be due to damage to the membrane of bacterial cells by hydrogen peroxide or to the affinity between zinc oxide nanoparticles and bacterial surfaces [58–61].

Based on the results obtained from the disc diffusion technique, it is clear that the fabricated PCL/ZnO nanocomposite membrane can successfully avoid bacterial growth at the implantation site.

Effects of Different Nanoparticle Concentrations on the Proliferation of Adult Goat Fibroblast Cells

The effects of ZnO nanoparticle concentration on cell proliferation are shown in Figs. 19, 20, and 21. From the visible observation of the membranes, it was clear that the color of the membrane changed from white to pale pink due to the attachment and proliferation of fibroblasts through the membrane (Fig. 19).

Both the membranes containing ZnO nanoparticles 0.5 % and 1 % appeared to be more pinkish due to the enhanced growth of cells (19(A) and 19(B)). In comparison with lower
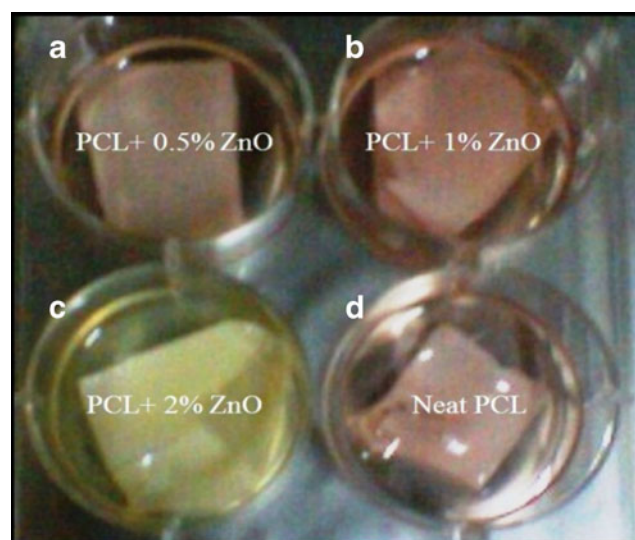
Table 2 Inhibition zone diameter from disc diffusion method

Sample	Inhibition zone diameter (mm)	
	E. coli	*S. aureus*
Neat PCL membrane	6.00±0	6.00±0
PCL/2 % ZnO	6.00±0	6.00±0
PCL/3 % ZnO	6.00±0	6.00±0
PCL/4 % ZnO	6.00±0	6.00±0
PCL/5 % ZnO	8.76±1.2	9.98±0.6
PCL/6 % ZnO	9.81±0.8	10.22±1.3

Fig. 19 Photograph showing the growth of adult goat fibroblast cells on the electrospun membranes after 24 h of culture. PCL membranes with 0.5 % ZnO nanoparticles (**a**), 1 % ZnO nanoparticles (**b**), 2 % ZnO nanoparticles (**c**) and the PCL membrane without nanoparticles (**d**)
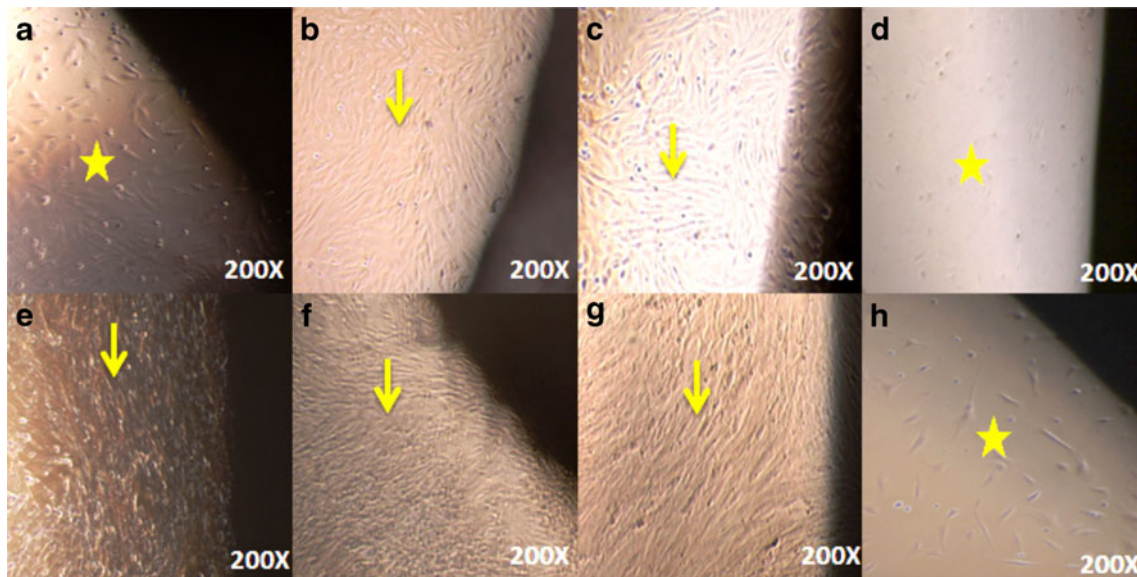
Fig. 20 Proliferation of adult goat fibroblast cells through the membranes. Neat PCL membranes (**a** and **e**), with 0.5 % ZnO nanoparticles (**b** and **f**), with 1 % ZnO nanoparticles (**c** and **g**), and with 2 % ZnO nanoparticles (d and h). The first row (**a**, **b**, **c**, and **d**) is after the cell culture of 24 h, and the second row is after 72 h of cell culture. *Arrows* indicate fibroblast cells and *stars* indicate membranes

concentrations of ZnO nanoparticles, concentrations of 2 % and above inhibited cell proliferation, and thus, the membranes seemed to be pale yellow. From the phase-contrast microscopic images, it is also clear that the PCL membranes containing 0.5 and 1 % ZnO nanoparticles enhanced cell proliferation more compared to the neat PCL membrane. After 24 h of incubation, a large number of fibroblast cells attached to and grew through the PCL membranes with 0.5 and 1 % ZnO nanoparticles, almost in the same manner. However, through the neat PCL membranes, only a small number of fibroblasts were able to grow. The PCL membrane containing 2 % ZnO nanoparticles considerably inhibited the proliferation of fibroblasts (Fig. 20(a–d)).

Fig. 21 Cell viability assay of fabricated membranes with different ZnO nanoparticle concentrations

A similar trend was observed even after 72 h of incubation (Fig. 20(e–h)). At this stage, the PCL membrane with 1 % ZnO nanoparticles showed higher cell attachment and proliferation (Fig. 20(g)). The fibroblasts particularly exhibited their elongated spindle-shaped morphology on the PCL membranes with 0.5 and 1 % ZnO nanoparticle content. It was observed that at a concentration of 1 % ZnO nanoparticles, the proliferation of fibroblast cells was significantly improved. Thus, lower ZnO nanoparticle concentration induces the growth and proliferation of fibroblast cells, whereas higher concentrations inhibit the proliferation of fibroblast cells on the membranes.

The enhanced proliferation of fibroblasts at lower concentrations of ZnO nanoparticles could be explained in terms of the role of reactive oxygen species (ROS) in cell replication, differentiation, and cell transcription [24–28]. It is well-established that the ZnO nanoparticles can produce ROS [29–33]. The ROS is a potential cue for cell proliferation, wound healing, and inflammation at low levels, however, it may damage the cells at higher levels. This might be the reason for the higher fibroblast proliferation at a relatively lower concentration of ZnO nanoparticles and the reduction in cell proliferation at higher concentrations. A recent report suggests that the studies on human dermal fibroblast cells (HDF) have shown more cells attached to chitosan bandages containing a lower concentration of ZnO nanoparticles, in comparison to those with a higher concentration [40].
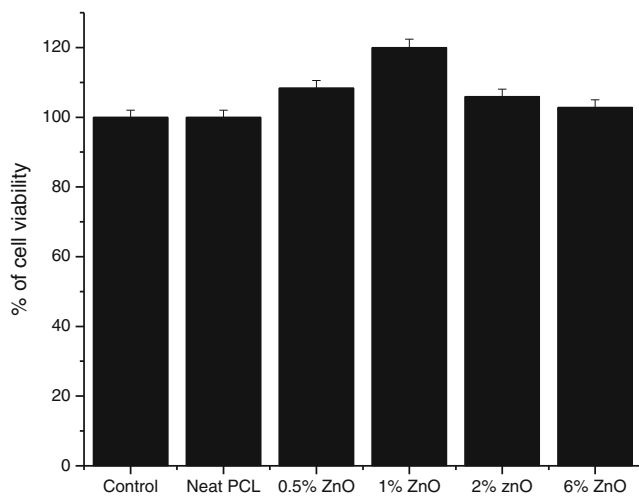
Cell Proliferation Assay on Adult Goat Fibroblast Cells

The effects of PCL membrane containing different concentrations of nanoparticles on the proliferation and viability of adult goat fibroblast cells were tested by MTX assay. The

absorbance was recorded in a NanoQuant microplate reader at a wavelength of 450 nm. Interestingly, none of the fabricated membranes showed any toxicity and all the membranes showed higher proliferation than the controls, with statistical significance. PCL with 0.5 % ZnO concentration possessed 108.37 ± 1.2 % ($P=0.0005$) cell viability . The membranes with ZnO nanoparticle concentration of 1 % showed the highest cell proliferation (120 ± 1.5 % with $P<0.0001$), and that containing 6 % concentration showed the least proliferation (103.7 ± 1.7 % with $P=0.0106$) in the MTX assay (Fig. 21). However, none of the membranes were cytotoxic, since all the membranes showed more than 100 % viability.

The studies on human dermal fibroblast cells (HDF) by Sudheesh et al. showed that the viability of cells was about 80–90 % with a lower concentration of ZnO nanoparticles, and that this was reduced to 50–60 % in chitosan bandages with higher concentrations of ZnO nanoparticles [40]. A recent report suggests that ZnO nanoflowers induced proliferation and migration of endothelial cells and led to the formation of new blood vessels [34].

Conclusions

In this study, electrospun membranes with varying fiber morphologies were successfully fabricated from polycaprolactone by varying the ZnO nanoparticle concentration. As the concentration of ZnO nanoparticles increased from 0.1 to 6 wt.%, both fiber diameter and fiber morphology varied greatly. EDX and FT-IR analysis confirmed the incorporation of ZnO nanoparticles into the PCL matrix. FT-IR analysis also revealed the nature of interaction between the polymer and the ZnO nanoparticles. XRD analysis of the PCL/ZnO membranes has shown that the higher loading of ZnO nanoparticles decreased the crystalline phase of PCL. The inherent elastic nature of the PCL changed to a brittle nature after the incorporation of ZnO nanoparticles. The fabricated material showed an overall good antimicrobial activity against both *E. coli* and *S. aureus,* which suggests the ability of the fabricated material to prevent bacterial proliferation at the implantation site. Finally, the fabricated membranes have shown excellent fibroblast cell attachment and proliferation. Thus, this material can be effectively used as tissue-engineering scaffold material, especially for the regeneration of damaged skin where antimicrobial and rigorous cell proliferation properties are essential.

Conflict of Interest The authors declare that they have no conflicts of interest.

References

1. Patrícia BM, Gabriela AS, Rui LR (2007) Adv Drug Deliv Rev 59: 207–233
2. MacArthur BD, Oreffo RO (2005) Nature 433:7021–7019
3. Mathieu H (2001) J Surf Interf Anal 32:3–9
4. Li WJ, Laurencin CT, Caterson EJ, Tuan RS, Ko FKJ (2002) Biomed Mater Res 60:613–621
5. Rajesh V, Dhirendra SK (2006) Int J Nanomedicine 1:15–30
6. Ikada YJR (2006) Soc Interf 3:589–601
7. Oh SH, Park IK, Kim JM, Lee JH (2007) Biomaterials 28:1664–1671
8. Sokolsky PM, Agashi K, Olaye A, Shakesheff K, Domb AJ (2007) Polymer carriers for drug delivery in tissue engineering. Adv Drug Deliv Rev 59:187–206
9. Thandavamoorthy S, Bhat GS, Tock RW, Parameswaran S, Ramkumar SSJ (2005) Appl Poly Sci 96:557–569
10. Kenawy ER, Bowlin GL, Mansfield K, Layman J, Simpson DG, Sanders EH, Wnek GEJ (2002) Control Release 81:57–64
11. Patcharaporn W, Neeracha S, Prasit P, Pitt S (2006) Macromol Biosci 6:70–77
12. Min BM, Jeong L, Nam YS, Kim JM, Park WH (2004) Int J Biol Macromol 34:281–288
13. Yoshimoto H, Shin YM, Terai H, Vacanti JP (2003) Biomaterials 24: 2077–2082
14. Seema A, Joachim H, Wendorff, Andreas G (2008) Polymer 49: 5603–5621
15. Leea KH, Kimb HY, Khilb MS, Rab YM, Lee DR (2003) Polymer 44:1287–1294
16. Cevat E, Dilhan M, Hongjun W (2008) Biomaterials 29:4065–4073
17. Luigi C, Paola L, Mario M, Orsolina P, Gianfranco P (2008) Biomacromolecules 9:1527–1534
18. Min BM, Jeong L, Nam YS, Kim JM, Kim JY, Park WH (2004) Intl J Biol Macromol 34:281–288
19. Li WJ, Tuli R, Okafor C, Derfoul A, Danielson KG, Hall DJ, Tuan RS (2004) Biomaterials 26:599–609
20. Li XH, Xing YG, Li WL, Jiang YH, Ding YL (2010) Food Sci Technol Int 16:225–232
21. Elen K, Murariu M, Peeters R, Dubois PH, Mullens J, Hardy A, Van Bael MK (2012) Polym Adv Technol 23:1422–1428
22. Aslan S, Loebick CZ, Kang S, Elimelech M, Pfefferle LD, Van Tassel PR (2010) Nanoscale 2:1789–1794
23. Vlad S, Ciobanu C, Gradinaru RV, Gradinaru LM, Nistor A (2011) Dig J Nanomater Bios 6:921–930
24. Thannickal VJ, Fanburg BL (2000) AJP - Lung Physiol 279: 6L1005–6L1028
25. Goldkorn T, Balaban N, Matsukuma K, Chea V, Gould R, Last J, Chan C, Chavez C (1998) Am J Respir Cell Mol Biol 19:786–798
26. Bryan N, Ahswin H, Smart N, Bayon Y, Wohlert S, Hunt JA (2012) Eur Cell Mater 24:249–265
27. Huo Y, Qiu WY, Pan Q, Yao YF, Xing K, Lou MF (2009) Exp Eye Res 89:876–886
28. Gamou S, Shimizu N (1995) FEBS Lett 357:161–164
29. Toduka Y, Toyooka T, Ibuki Y (2012) Environ Sci Technol 46:7629–7636
30. Guo D, Bi H, Liu B, Wu Q, Wang D, Cui Y (2012) Toxicol In Vitro 27:731–738
31. Dutta RK, Nenavathu BP, Gangishetty MK, Reddy AV (2012) Colloids Surf B 94:143–150
32. Ashutosh K, Alok KP, Shashi SS, Rishi S, Alok D (2011) Free Radical Bio Med 51:1872–1881
33. Mariappan P, Krishnamoorthy K, Kadarkaraithangam J, Govindasamy M (2011) Nanomed-Nanotechnol 7:184–192
34. Barui AK, Veeriah V, Mukherjee S, Manna J, Patel AK, Patra S, Pal K, Murali S, Rohit KR, Chatterjee S, Patra CR (2012) Nanoscale 4: 7861–7869

35. Brandaˆo-Neto J, Stefan V, Mendoc BB, Bloise W, Castro AV (1995) Nutr Res 15:335–358
36. Salgueiro MJ, Zubillaga MB, Lysionek AE, Caro RA, Weill R, Boccio JR (2012) Nutrition 18:510–519
37. Fujiwara Y, Kaji T (1997) Res Commun Mol Pathol Pharmacol 97:95–106
38. Newell KJ, Witty JP, Rodgers WH, Matrisian LM (1994) Mol Carcinogen 10:199–120
39. Mack CF, Knox JD, Powell WC, Nagle RB, Bowden GT (1993) Int J Radiat Oncol 27:217
40. Sudheesh Kumar PT, Vinoth KL, Mincy R, Raja B, Tamura H, Nair SV, Jayakumar R (2013) Pharm Res 523-537
41. Silke M, Jean SS, Bruce CD, John FR (2002) Macromolecules 35:8456–8466
42. Fashandi H, Karimi M (2012) Polymer 53:5832–5849
43. Park MS, Kim JK (2004) Langmuir 20(13):5347–5352
44. Srinivasarao M, Collings D, Philips A, Patel S (2001) Science 292(5514):79–83
45. Francois B, Pitois O, Francois J (1995) Adv Mater 7(12):1041–1044
46. Limaye AV, Narhe RD, Dhote AM, Ogale SB (1996) Phys Rev Lett 76(20):3762–3765
47. Peng J, Han Y, Yang Y, Li B (2004) Polymer 45(2):447–452
48. Guiping M, Dongzhi Y, Jun N (2009) Polym Adv Technol 20:147–150
49. Zong XH, Kim K, Fang DF, Ran SF, Hsiao BJ, Chu BJ (2002) Polymer 43:4403–4412
50. Baumgarten PKJ (1971) Colloid Interf Sci 36:71–79
51. Fong H, Chun I, Reneker DH (1999) Polymer 40:4585–4592
52. Doshi J, Reneker DHJ (1995) Electrostatics 35(2–3):151–160
53. Li ZH, Su GY, Wang XY, Gao D (2005) S Solid State Ion 176:1903–1908
54. Lim CT, Tan EPS, Ng SY (2008) Appl Phys Lett 92:141908–141910
55. Moniruzzaman M, Chattopadhyay J, Billups WE, Winey KI (2007) Nano Lett 7:1178–1185
56. Reddy KM, Kevin F, Jason B, Denise GW, Cory H, Alex PJ (2007) Appl Phys Lett 90(21):1–3
57. Selahattin A, Kadri G, Ramazan C (1998) Tr J Med Sc 28:595–597
58. Sawai J, Kawada E, Kanou F, Igarashi H, Hashimoto A, Kokugan T, Shimizu MJ (1996) Chem Eng Jpn 29:627–633
59. Sawai J, Igarashi H, Hashimoto A, Kokugan T, Shimizu MJ (1996) Chem Eng Jpn 29:251–256
60. Yamamoto O (2001) Int J Inorg Mater 3:643–646
61. Stoimenov PK, Klinger RL, Marchin GL, Klabunde KJ (2002) Langmuir 18:6679–6686